9

Magnetic Damping Using Static Fields

> Science is nothing without generalisations. Detached and ill-assorted facts are only raw material, and in the absence of a theoretical solvent, have little nutritive value. At the present time and in some departments, the accumulation of material is so rapid that there is a danger of indigestion.
>
> *Rayleigh (1884)*

We have seen that the relative movement of a conducting body and a magnetic field can lead to the dissipation of energy. This has been used by engineers for over a century to dampen unwanted motion. Indeed, as far back as 1873 we find Maxwell noting: '*A metallic circuit, called a damper, is sometimes placed near a magnet for the express purpose of damping or deadening its vibrations.*' Maxwell was talking about a magnetic field moving through a stationary conductor. We are interested in a moving conductor in a stationary field, but of course, this is really the same thing. We have already touched upon magnetic damping in Chapter 5, and we discussed some of its consequences in Chapter 6. In particular, we saw that the intense magnetic field in a sunspot locally deadens the convective motions in the outer layer of the sun, thus cooling the spot and giving it a dark appearance. Here we make the jump from sunspots to steelmaking, and describe how magnetic fields are used in certain casting operations to suppress unwanted motion.

There has been a myriad of papers on this topic and at times one is reminded of Rayleigh's *indigestion*. Here we focus on the unifying themes. We shall see that the hallmark of magnetic damping is that the dissipation of energy is subject to the constraint of *conservation of momentum*, and that this constraint is a powerful one.

9.1 Metallurgical Applications

We have already seen that a static magnetic field can suppress motion of an electrically conducting liquid. The mechanism is straightforward: the motion of a liquid across the magnetic field lines induces a current. This leads to Joule dissipation and the resulting rise in

thermal energy is accompanied by a fall in magnetic and/or kinetic energy. We are concerned here only with cases where the magnetic Reynolds number is small, so that changes to the applied magnetic field are negligible. In such cases, the rise in Joule dissipation is matched by a fall in kinetic energy. Thus, for example, in an electrically insulated pool, (5.7) gives

$$\frac{d}{dt}\int\left(\frac{1}{2}\rho\mathbf{u}^2\right)dV = -\frac{1}{\sigma}\int\mathbf{J}^2 dV + \text{viscous dissipation}$$

In the last decade this phenomenon has been exploited in a range of metallurgical processes. For example, in the continuous casting of large steel slabs, an intense, static magnetic field (of around 0.5 Tesla) is commonly used to suppress motion within the mould (Figure 9.1). Sometimes the motion takes the form of a submerged jet which feeds the mould from above; at others it takes the form of large eddies or vortices. In both cases the objective is to keep the free surface of the liquid quiescent, thus avoiding the entrainment of surface debris (see Iron & Steel Institute of Japan, 1994.) In other solidification processes, such as the Bridgeman technique for growing semi-conductor crystals or the continuous casting of aluminium, it is widely believed that natural convection has a detrimental effect on the metallurgical structure of the solid. Again, the imposition of a static magnetic field is seen as one means of suppressing these unwanted motions (Muller, Neumann & Weber, 1984). This is discussed in Section 5 of this chapter. Finally, magnetic damping is used in the laboratory measurements of chemical and thermal diffusivities, particu-

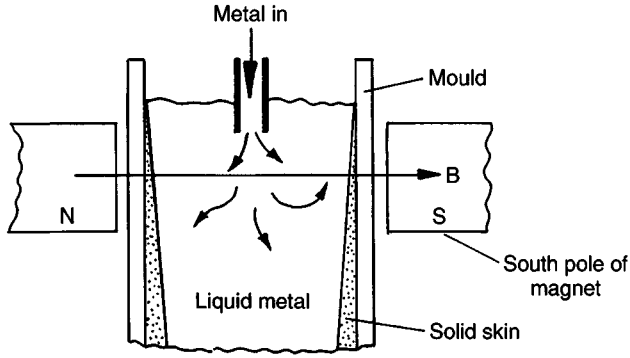

Figure 9.1 Magnetic damping is used to suppress motion in the continuous casting of steel slabs.

larly where solutal or thermal buoyancy can disrupt the measurement technique (Nakamura et al., 1990). For example, in the 'hot-wire' technique for measuring the thermal conductivity of liquid metals, the conductivity is determined by monitoring the rate at which heat diffuses into the liquid from a long, thin, vertical wire. This technique relies on conduction being dominant over convection. Yet natural convection is always present to some degree in the form of a buoyant plume. The simplest way of suppressing the unwanted motion is magnetic damping (Figure 9.2(a)).

In this chapter we examine the magnetic damping of jets, vortices and natural convection. Our aim is to present a unified theoretical framework from which the many disparate published studies may be viewed. We shall see that the hallmark of magnetic damping is that mechanical energy is destroyed while momentum is conserved. It is this need to conserve momentum, despite the dissipation of energy, which gives magnetic damping its special character.

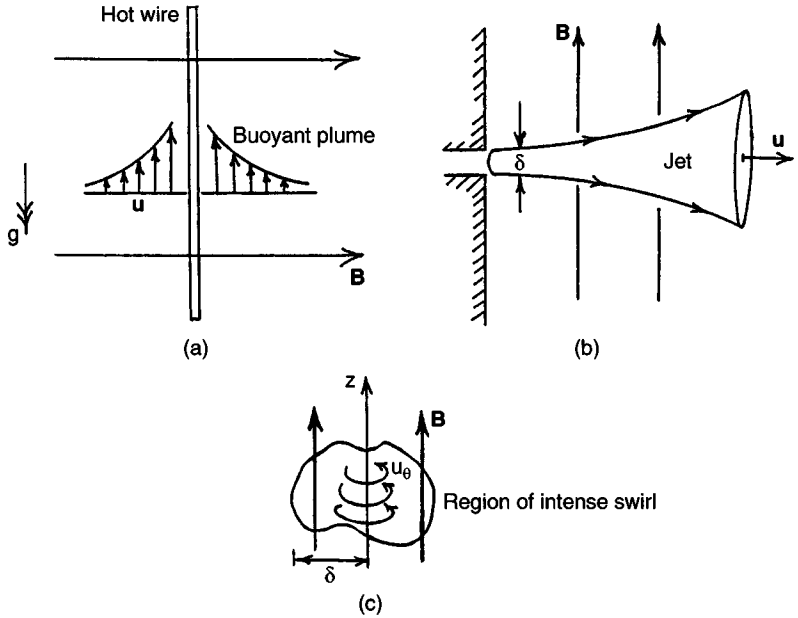

Figure 9.2 Examples of magnetic damping of liquid-metal flows. (a) A buoyant plume is generated by a hot wire and suppressed by an imposed field. (b) A jet is created by side-wall injection at the boundary. (c) A magnetic field dissipates an isolated vortex.

9.2 Conservation of Momentum, Destruction of Energy and the Growth of Anisotropy

We consider flows in which the Reynolds number is large and the magnetic field induced by currents flowing in the liquid is much smaller than the externally imposed field. This covers most laboratory and industrial applications. In view of the large Reynolds number, we may treat the motion as inviscid, except of course when it comes to the small-scale components of turbulence. In the interests of simplicity we take $\mathbf{B}$ to be uniform, imposed in the z-direction, and consider domains which are infinite in extent or else bounded by an electrically insulated surface.

Since $\mathbf{B}$ is fixed and uniform, Faraday's equation demands that $\nabla \times \mathbf{E} = 0$. Ohm's law then takes the form

$$\mathbf{J} = \sigma(-\nabla\Phi + \mathbf{u} \times \mathbf{B}) \tag{9.1a}$$

where Φ is the electrostatic potential and $\mathbf{B}$ is the uniform, imposed magnetic field. Now we also know, from Ampère's law, that $\mathbf{J}$ is solenoidal and so we have

$$\nabla \cdot \mathbf{J} = 0, \qquad \nabla \times \mathbf{J} = \sigma \mathbf{B} \cdot \nabla \mathbf{u} \tag{9.1b}$$

Equations (9.1b) uniquely determine $\mathbf{J}$. (Recall that a vector field is uniquely determined if its divergence and curl are specified.) The key point is that $\mathbf{J}$ is zero if and only if $\mathbf{u}$ is independent of z. Now the Lorentz force per unit mass, $\mathbf{J} \times \mathbf{B}/\rho$, is readily obtained from (9.1a):

$$\mathbf{F} = -\frac{\mathbf{u}_\perp}{\tau} + \frac{\sigma(\mathbf{B} \times \nabla\Phi)}{\rho}, \qquad \tau = \rho/\sigma B^2 \tag{9.2}$$

Here $\mathbf{u}_\perp = (u_x, u_y, 0)$ and τ is the Joule damping term. Note that the first term in (9.2) looks like a linear friction term. However, this expression for $\mathbf{F}$ is awkward as it contains the unknown potential Φ. This potential is given by the divergence of Ohm's law (9.1a), which yields $\Phi = \nabla^{-2}(\mathbf{B} \cdot \boldsymbol{\omega})$ (here $\boldsymbol{\omega}$ is the vorticity field.) Clearly, when $\mathbf{B}$ and $\boldsymbol{\omega}$ are mutually perpendicular, the Lorentz force simplifies to $-\mathbf{u}_\perp/\tau$, and so (pressure forces apart) $\mathbf{u}_\perp$ declines on a time scale of τ. This is the phenomenological basis of magnetic damping. Loosely speaking, we may think of rotational motion being damped out provided that its axis of rotation is perpendicular to $\mathbf{B}$. The ratio of the damping time, τ, to the characteristic advection time, l/u, gives the interaction parameter

$$N = \sigma B^2 l/\rho u$$

Typically, N is indicative of the relative sizes of the Lorentz and inertial forces.

We now consider the rôle of Joule dissipation. This provides an alternative way of quantifying magnetic damping. The inviscid equation of motion

$$\frac{D\mathbf{u}}{Dt} = -\nabla\left(\frac{p}{\rho}\right) + \mathbf{F}, \qquad \mathbf{F} = \mathbf{J} \times \mathbf{B}/\rho$$

yields the energy equation

$$\frac{dE}{dt} = -\frac{1}{\rho\sigma}\int \mathbf{J}^2 dV = -D \tag{9.3}$$

where D is the Joule dissipation rate and E is the global kinetic energy. Clearly, E declines until $\mathbf{J}$ is zero, which happens only when $\mathbf{u}$ is independent of z. We can use (9.3) to estimate the rate of decline of energy. Let $l_{//}$ and $l_{\min}$ be two characteristic length scales for the flow, the first being parallel to $\mathbf{B}$. Then $\nabla \times \mathbf{J}$, and hence $|\mathbf{J}| \sim l_{\min}\nabla \times \mathbf{J}$, may be estimated from (9.1b), and this yields

$$\frac{dE}{dt} = -D \sim -\left(\frac{l_{\min}}{l_{//}}\right)^2 \frac{E}{\tau} \tag{9.4a}$$

from which

$$E \sim E_0 \exp\left[-\tau^{-1}\int_0^t \left(l_{\min}/l_{//}\right)^2 dt\right] \tag{9.4b}$$

The implication is that, provided $l_{\min}$ and $l_{//}$ remain of the same order, the flow will be destroyed on a time scale of τ. Indeed, this might have been anticipated from (9.2). However, this is not the end of the story. The dissipation is subject to some powerful integral constraints. The key point is that $\mathbf{F}$ cannot create or destroy linear momentum, nor (one component of) angular momentum. For example, since $\mathbf{J}$ is solenoidal,

$$\rho\int \mathbf{F} dV = -\mathbf{B} \times \int \mathbf{J} dV = 0 \tag{9.5}$$

Thus the Lorentz force cannot itself alter the global linear momentum of the fluid. Similarly, following Davidson (1995), we have

$$(\mathbf{x} \times \mathbf{F}) \cdot \mathbf{B} = \rho^{-1}[(\mathbf{x} \cdot \mathbf{B})\mathbf{J} - (\mathbf{x} \cdot \mathbf{J})\mathbf{B}] \cdot \mathbf{B} = -\left(B^2/2\rho\right)\nabla \cdot \left[\mathbf{x}_\perp^2 \mathbf{J}\right] \tag{9.6}$$

which integrates to zero over the domain (see also the discussion in Chapter 5, Section 3). Evidently, the Lorentz force has zero net torque parallel to $\mathbf{B}$, and so cannot create or destroy the corresponding compo-

nent of angular momentum. The physical interpretation of (9.6) is that **J** may be considered to be composed of many current tubes, and that each of these tubes may, in turn, be considered to be the sum of many infinitesimal current loops, as in the proof of Stokes' theorem. However, the torque on each elementary current loop is $(d\mathbf{m}) \times \mathbf{B}$, where $d\mathbf{m}$ is its dipole moment. Consequently, the global torque, which is the sum of many such terms, can have no component parallel to **B**.[1]

Now the fact that **F** cannot create or destroy linear momentum, nor one component of angular momentum, would not be important if the mechanical forces themselves changed these momenta. However, in certain flows, such as submerged jets, the mechanical (pressure) forces cannot alter the linear momentum of the fluid. In others, such as flow in an axisymmetric container, the pressure cannot alter the axial component of angular momentum. In such cases there is always some component of momentum which is conserved, despite the Joule dissipation. This implies that the flow cannot be destroyed on a time scale of τ, and from (9.4) we may infer that $l_{//}/l_{\min}$ must increase with time. We might anticipate, therefore, that these flows will exhibit a pronounced anisotropy, with $l_{//}$ increasing as the flow evolves, and indeed, this is exactly what happens. These results are summarised in Table 9.1.

Of course, it has been known for a long time that a strong magnetic field promotes two-dimensional turbulence. However, the traditional explanation is rather different from that given above, and so is worth repeating here. If $\nabla \times \mathbf{F}$ is evaluated from (9.2) and substituted into the vorticity equation, we obtain

$$\frac{D\boldsymbol{\omega}}{Dt} = \boldsymbol{\omega} \cdot \nabla \mathbf{u} - \frac{1}{\tau} \nabla^{-2} \left[\partial^2 \boldsymbol{\omega} / \partial z^2 \right] \tag{9.7}$$

(Roberts, 1967). Phenomenologically, we might consider ∇^{-2} to be replaced by $-l_{\min}^2$, in which case the Lorentz term promotes a unidirectional diffusion of vorticity along the **B**-lines, with a diffusivity of $l_{\min}^2/\tau$. For cases where $l_{//} \gg l_{\min}$, this may be made rigorous by taking the two-dimensional Fourier transform of (9.7) in the x–y plane. This argument is a powerful one when N is large, so that the non-linear inertial terms are negligible. However, when N is small or moderate, the vortex lines stretch and twist on a time scale of l/u, which is smaller than, or of the order of, τ. In such cases it is difficult to infer much from (9.7) and there is an advantage in returning to the integral arguments given above.

[1] Private communication, S. Davidson, 1993.

Table 9.1. *The 'rules' of magnetic damping*

Quantity	Equation	Implication
Energy	$\frac{dE}{dt} = -\frac{1}{\rho\sigma}\int \mathbf{J}^2 dV \sim -\left(\frac{l_{\min}}{l_{//}}\right)^2 \frac{E}{\tau}$	If E is to remain finite then $l_{//}$ must grow relative to $l_{\min}$. Some form of anisotropy then develops
Global Lorentz force	$\int \mathbf{J} \times \mathbf{B}_0 dV = 0$	Linear momentum is neither created nor destroyed by the Lorentz force
Global Lorentz torque	$\int [\mathbf{x} \times (\mathbf{J} \times \mathbf{B}_0)]_{//} dV = 0$	The parallel component of angular momentum is neither created nor destroyed by the Lorentz force

9.3 Magnetic Damping of Submerged Jets

We are interested here in the dissipation of submerged jets such as that shown in Figure 9.2(b). However, we start with the slightly artificial problem of a long, uniform jet which is dissipated by the sudden application of a magnetic field. This provides a useful stepping stone to the more important problem of a submerged jet which evolves in space, rather than in time.

Suppose that we have a unidirectional jet, $\mathbf{u} = u(x, z, t)\hat{\mathbf{e}}_y$, which is initially axisymmetric (Figure 9.3a). At $t = 0$ we impose a uniform magnetic field in the z-direction. Current will be induced as shown in Figure 9.3(b), driven parallel to x by $\mathbf{u} \times \mathbf{B}$, but forced to recirculate back through regions of weak or zero flow by the electrostatic potential. Since the current is two-dimensional, we may introduce a streamfunction, ψ, for $\mathbf{J}$ which is related to $\mathbf{u}$ by Ohm's law.

$$\mathbf{J} = \nabla \times [\psi \hat{\mathbf{e}}_y], \qquad \nabla^2 \psi = -\sigma B \frac{\partial u}{\partial z} \tag{9.8}$$

Our equation of motion is then

$$\frac{\partial u}{\partial t} = \frac{B}{\rho}\frac{\partial \psi}{\partial z} = -\frac{1}{\tau}\nabla^{-2}\left[\frac{\partial^2 u}{\partial z^2}\right] \tag{9.9}$$

Evidently, linear momentum is conserved, since $\partial\psi/\partial z$ integrates to zero. Now let δ be the thickness of the jet in the x-direction and $l_{//}$ be the characteristic lengthscale for u parallel to $\mathbf{B}$.

Then, from conservation of momentum, in conjunction with energy equation (9.4a), we have

$$\frac{dE}{dt} = -\left(\frac{\delta}{l_{//}}\right)^2 \frac{E}{\tau}, \qquad E = u^2 l_{//}\delta, \qquad u l_{//}\delta = \text{constant} \tag{9.10}$$

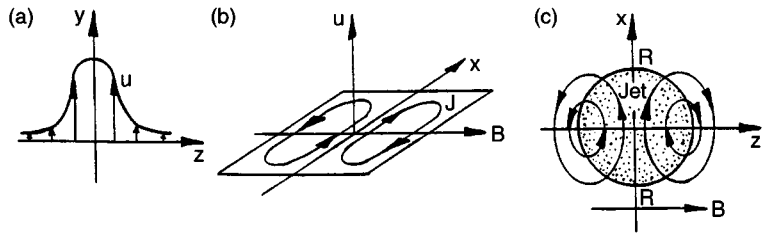

Figure 9.3 Magnetic damping of a jet: (a) initial axisymmetric velocity profile; (b) the induced current; (c) cross-section through the jet. A reverse flow forms at points marked R.

Clearly, $l_{//}/\delta$ must increase with time. If it did not, then E would decline exponentially, which is forbidden by conservation of momentum. For fixed δ the only possible solutions to (9.10) are (Davidson, 1995)

$$l_{//} \sim \delta(t/\tau)^{1/2}, \qquad u \sim u_0(t/\tau)^{-1/2} \tag{9.11}$$

Thus the flow spreads laterally along the field lines, evolving from a jet into a sheet. The mechanism for this lateral spreading is evident from Figure 9.3. The induced currents within the jet give rise to a braking force, as expected. However, the current which is recycled either side of the jet actually accelerates previously stagnant fluid at large $|z|$. Hence the growth in $l_{//}$. Notice also, that at points marked R a counterflow will be generated since **F** points in the negative y-direction and u is initially zero.

The existence of a counterflow, as well as the scaling laws (9.11), are readily confirmed by exact analysis. For example, taking the Fourier transform of (9.9) leads to an exact solution in terms of hypergeometric functions, as we now show. Let U be the cosine transform of u. Then

$$U(k_x, k_z) = 4\int_0^\infty \int_0^\infty u(x, z)\cos(xk_x)\cos(zk_z)dxdz$$

Our equation of motion (9.9) transforms to

$$\frac{\partial U}{\partial t} + \cos^2\phi\frac{U}{\tau} = 0, \qquad \cos\phi = k_z/k$$

where $k^2 = k_x^2 + k_z^2$. Solving for U and taking the inverse transform yields

$$u(\mathbf{x}, t) = \pi^{-2}\int_0^\infty \int_0^{\pi/2} e^{-(\cos^2\phi)\hat{t}}\cos(xk_x)\cos(zk_z)U_0(k)kdkd\phi$$

Here $\hat{t}$ is the scaled time, t/τ and $U_0(k)$ is the transform of the initial axisymmetric velocity profile, $u_0(r)$. For large t this can be simplified using the relationship

$$\int_0^\infty e^{-p^2}\cos(\lambda p)dp = (\sqrt{\pi}/2)e^{-\lambda^2/4}$$

to give

$$u(\mathbf{x}, t) = \frac{1}{2\pi\sqrt{\pi\hat{t}}}\int_0^\infty e^{-k^2z^2/4\hat{t}}\cos(xk)U_0(k)kdk$$

(This is left as an exercise for the reader.) It is clear from this integral that, for large t, u must be of the form

$$u(\mathbf{x}, t) \sim \hat{t}^{-1/2} F(z/\hat{t}^{1/2}, x)$$

which confirms the scaling laws (9.11). Of course, the form of F depends on the initial conditions. For example, if we take $u_0(r) = V \exp(-r^2/\delta^2)$, $r^2 = x^2 + z^2$, then the integral above yields

$$u(\mathbf{x}, t) = \frac{V}{\sqrt{\pi \hat{t}}} \frac{G(\zeta)}{[1 + z^2/(\delta^2 \hat{t})]}, \qquad \zeta = \frac{x^2}{\delta^2 + z^2/\hat{t}}$$

where $G(\zeta)$ is Kummer's hypergeometric function, $G(\zeta) = M(1, \frac{1}{2}, -\zeta)$. An examination of the shape of $G(\zeta)$ confirms that a reverse flow develops, as anticipated in Figure 9.3.

Consider now a submerged, steady jet evolving in space, rather than in time. This is illustrated in Figure 9.4. It is generated by injecting fluid through a circular aperture in a side wall and into a uniform magnetic field. We consider the case where **B** is weak (N is small) so that the jet inertia is much larger than the Lorentz force. This configuration is particularly relevant to the magnetic damping of jets in castings.

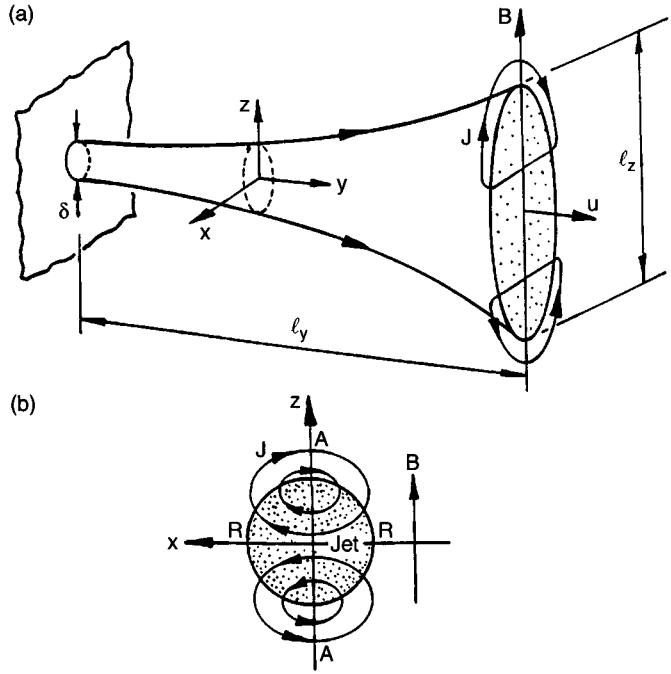

Figure 9.4 MHD jet produced by side-wall injection: (a) spatial evolution of jet; (b) the current paths. A reverse flow occurs at points marked R.

Since N is small, the magnetic field influences the jet only slowly. As a result, the characteristic axial length scale of the jet, l_y, is much greater than l_x and l_z. Now the current must form closed paths. However, each cross section of the jet looks very much like its neighbouring cross sections, and so the current must close in the (x,z)-plane, just as it did in the previous example. Figure 9.4 illustrates the situation. As before, the induced current recirculates through regions of weak or zero flow. It follows that a reverse flow will form at points marked R, and momentum will diffuse out along the z-axis by precisely the same mechanism as before. Thus the jet cross section becomes long and elongated. Now if the jet is to spread laterally along the **B**-lines, then continuity of mass requires that there is some entrainment of the surrounding fluid. (We shall confirm this shortly.) We would expect, therefore, that the jet draws in fluid from the far field, predominantly at large $|z|$. Conversely, regions of reverse flow on the x-axis will produce an outward flow of mass near the wall (Figure 9.5). This complex three-dimensional flow pattern was proposed independently by Davidson (1995), based on theoretical considerations, and by Harada et al. (1994), based on experimental observations.

We now confirm this picture using the Euler equation. The equation of motion for the jet is very similar to (9.9). In terms of the streamfunction ψ, we have

$$\frac{Du_y}{Dt} = \mathbf{u} \cdot \nabla u_y = \frac{B}{\rho}\frac{\partial \psi}{\partial z} = -\frac{1}{\tau}\nabla^{-2}\left[\frac{\partial^2 u_y}{\partial z^2}\right] \tag{9.12}$$

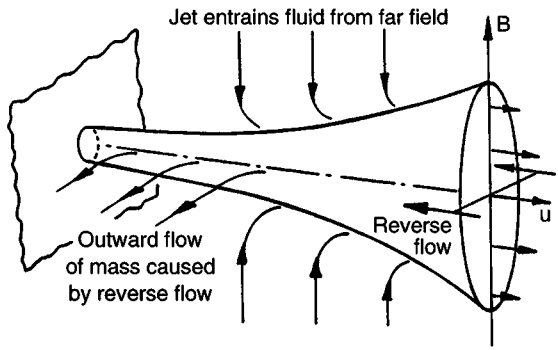

Figure 9.5 MHD jet produced by side-wall injection. The jet draws in fluid from the far field and the reverse flow produces on outward flow of mass near the wall.

Unlike (9.9), this is non-linear, and so exact solutions are unlikely to be found. However, we may still use conservation of momentum in conjunction with an energy dissipation equation. Let M be the momentum flux in the jet, $M = \int u_y^2 dA$. From (9.12) this is conserved. Also from (9.12) we can construct an energy equation reminiscent of (9.4a).

$$\frac{d}{dy}\int\left(\frac{1}{2}u_y^3\right)dA = -\frac{1}{\rho\sigma}\int \mathbf{J}^2 dA$$

It follows that u_y and $l_{//}$ scale as (Davidson, 1995)

$$u_y \sim \left[\frac{\tau M^2}{\delta^4 y}\right]^{1/3}, \qquad l_{//} \sim \left[\frac{\delta^5 y^2}{\tau^2 M}\right]^{1/3} \tag{9.13}$$

(It is readily confirmed that these are the only scalings which satisfy $M =$ constant as well as the energy equation above.) Note that mass flux in the jet increases with y, as shown in Figure 9.5.

It is interesting to compare (9.13) and Figure 9.5 with the two-dimensional jet analysed in Chapter 5, Section 2.2. Evidently a two-dimensional jet, where the current paths do not close in the fluid, behaves quite differently from a three-dimensional jet. Of course, it is the three-dimensional jet which is the more important in practice.

9.4 Magnetic Damping of Vortices

9.4.1 General considerations

So far we have considered only cases where the conservation of linear momentum provides the key integral constraint. We now consider examples where conservation of angular momentum is important, i.e. vortices. The discussion is restricted to inviscid fluids. Suppose we have one or more vortices, of arbitrary orientation, held in a spherical domain. Then, as we saw in Chapter 5, Section 3, the global magnetic torque is given by

$$\mathbf{T} = \frac{1}{\rho}\int \mathbf{x}\times(\mathbf{J}\times\mathbf{B})d\mathrm{V} = -\frac{1}{4\tau}\int(\mathbf{x}\times\mathbf{u})_\perp d\mathrm{V} \tag{9.14}$$

(This holds for any distribution of $\mathbf{u}$.) If $\mathbf{H}$ is the global angular momentum of the fluid, then (9.14) gives the inviscid equation of motion

$$\frac{\partial \mathbf{H}}{\partial t} = -\frac{\mathbf{H}_\perp}{4\tau}$$

It follows that $\mathbf{H}_{//}$ is conserved while $\mathbf{H}_{\perp}$ declines exponentially (Davidson, 1995):

$$\mathbf{H}_{//} = \text{constant}; \qquad \mathbf{H}_{\perp}(t) = \mathbf{H}_{\perp}(0)\exp[-t/4\tau] \tag{9.15a, b}$$

The simplicity of this result is rather surprising, particularly as it applies for any value of N, and so is valid even when inertia is dominant and the stretching and twisting of vorticity is more vigorous than the damping. Now the conservation of $H_{//}$ gives us a lower bound on E:

$$E \geq H_{//}^2 \left[2 \int \mathbf{x}_{\perp}^2 dV \right]^{-1} \tag{9.16}$$

This, in conjunction with the energy equation

$$\frac{dE}{dt} = -\frac{1}{\rho\sigma} \int J^2 dV$$

provides a powerful constraint on the way in which these flows evolve. Typically, the energy of the flow decreases through the destruction of $\mathbf{H}_{\perp}$ until only $\mathbf{H}_{//}$ remains. Since there is a lower bound on E, it follows that the flows must eventually evolve to a state in which $\mathbf{u}$ is finite, but $\mathbf{J}$ is everywhere zero. From (9.1b) it is clear that the final motion must be two-dimensional (Figure 9.6), $\mathbf{u} = \mathbf{u}(x, y)$ consisting of one or more columnar vortices which span the sphere and whose axes are parallel to $\mathbf{B}$. A natural question to ask is: how do the vortices evolve into these long columnar structures? We would expect the initial evolution of a small vortex to be independent of the shape of the remote boundaries, and so we now dispense with the spherical boundary and consider vortices in

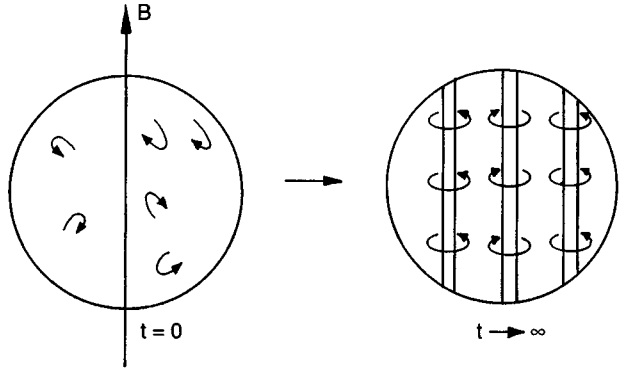

Figure 9.6 Inviscid flow in a sphere which is subject to a uniform field always evolves towards a two-dimensional state.

infinite (or else large, but finite) domains. There are two special cases which deserve particular attention. One is where the vorticity is aligned with **B**, and the other is where **B** and ω are mutually perpendicular. We start with transverse vortices.

9.4.2 *Damping of transverse vortices*

In the interests of simplicity we shall consider a two-dimensional vortex whose axis is normal to the imposed magnetic field. Suppose our flow is confined to the (x,z)-plane and bounded by the cylindrical surface $x^2 + z^2 = R^2$. We are interested particularly in isolated vortices whose characteristic radius, δ, is much less than R. We shall take the vortex to be initially axisymmetric and subject to a uniform magnetic field, **B**, imposed in the z-direction (see Figure 9.7). Once again, we shall find that global angular momentum provides the key to determining the evolution of the flow.

Since **B** and ω are mutually perpendicular the electrostatic potential is zero (c.f. $\Phi = \nabla^{-2}(\mathbf{B}\cdot\omega)$), and so (9.2) gives the Lorentz force and magnetic torque as

$$\mathbf{F} = -(u_x/\tau)\hat{\mathbf{e}}_x, \qquad T_y = -\tau^{-1}\int zu_x dV = -H_y/2\tau \qquad (9.17, 9.18)$$

Here H_y is the global angular momentum, which may be expressed either in terms of u or else in terms of the two-dimensional streamfunction, ψ:

$$H_y = \int (zu_x - xu_z)dV = 2\int zu_x dV = 2\int \psi dV$$

It follows immediately that, even in the low N (non-linear) regime, the angular momentum decays in a remarkably simple manner:

$$H_y(t) = H_y(0)e^{-t/2\tau} \qquad (9.19)$$

This is the two-dimensional counterpart of (9.15). It is tempting to conclude, therefore, that the vortex decays on a time-scale of 2τ. However, this appears to contradict (9.7) which, in the present context, simplifies to

$$\frac{D\omega}{Dt} = -\frac{1}{\tau}\nabla^{-2}\left[\partial^2\omega/\partial z^2\right] \qquad (9.20)$$

We may write this in the form

$$\frac{D\omega}{Dt} \sim \frac{\delta^2}{\tau}\frac{\partial^2\omega}{\partial z^2}$$

and anticipate (correctly) that there is a continual diffusion of vorticity along the z-axis. In the limit of large N we have the simple diffusion equation

$$\frac{\partial \omega}{\partial t} \sim \frac{\delta^2}{\tau} \frac{\partial^2 \omega}{\partial z^2} \tag{9.21}$$

which suggest that the cross section of the vortex distorts from a circle to a sheet on a time-scale of τ. If this picture is correct, and we shall see that it is, this distortion should proceed in accordance with

$$l_z \sim \delta(t/\tau)^{1/2} \tag{9.22}$$

This elongation of the eddy will cease only when the influence of the boundary is felt. We therefore have two conflicting views. On the one hand, (9.19) suggests that the flow is destroyed on a time-scale of 2τ. On the other, (9.22) suggests a continual evolution of the vortex until such time as the boundary plays an important rôle. This will occur when $l_z \sim R$, which requires a time of the order of $(R/\delta)^2\tau$. We shall now show how these two viewpoints may be reconciled.

We consider the linear case where the magnetic field is relatively intense, so that $N \gg 1$. We further simplify the problem by insisting that the boundaries are remote ($R \gg \delta$) so that we may consider flow in an infinite domain. This greatly simplifies the algebra, but at a cost. In order that all relevant integrals converge, particularly the angular momentum, we require that the integral of ψ converges, and this limits our possible choice of initial conditions. However, this sub-class of flows will suffice to show the general behaviour.

Let us introduce the Fourier transform

$$\Psi(k_x, k_z) = 4 \int_0^\infty \int_0^\infty \psi(x, z) \cos(xk_x) \cos(zk_z) dx dz \tag{9.23}$$

and apply this transform to (9.20), rewritten as

$$\frac{\partial \psi}{\partial t} = -\frac{1}{\tau} \nabla^{-2} \frac{\partial^2 \psi}{\partial z^2} \tag{9.24}$$

Let $\hat{t}$ be the dimensionless time t/τ, k the magnitude of $\boldsymbol{k}$, and Ψ_0 the transform of ψ at $t = 0$. Then the transformed version of (9.24) is readily integrated to give $\Psi = \Psi_0(k) e^{-(\cos^2\phi)\hat{t}}$; $\cos\phi = k_z/k$. However, this is identical to the solution we obtained for a two-dimensional jet in Section 9.3. Thus, without any further work, we may say that at large times

$$\psi(\mathbf{x}, t) = \frac{1}{2\pi(\pi\hat{t})^{1/2}} \int_0^\infty e^{-k^2 z^2/4\hat{t}} \cos(xk_x)\Psi_0(k)kdk \tag{9.25}$$

Evidently, for $t \gg \tau$, $\psi(\mathbf{x}, t)$ adopts the form

$$\psi(\mathbf{x}, t) \sim \hat{t}^{-1/2} F\left(z/\hat{t}^{1/2}, x\right) \tag{9.26}$$

where F is determined by the initial conditions. It would appear, therefore, that the arguments leading to (9.22) are substantially correct. An initially axisymmetric vortex progressively distorts into a sheet-like structure, with a longitudinal length scale given by (9.22). Note that (9.26) implies that $u_x \ll u_z$ while $u_z \sim \hat{t}^{-1/2}$. It follows that the kinetic energy of the eddy is progressively 'channelled' into the z-component of motion, and that the energy, E, declines as $E \sim (t/\tau)^{-1/2}$.

Let us now consider a specific example. Suppose that the initial eddy structure is described by

$$\psi_0(r) = \Phi_0 e^{-r^2/\delta^2}, \qquad r^2 = x^2 + z^2 \tag{9.27}$$

Then (9.25), which is valid for large t, may be integrated to give

$$\psi(\mathbf{x}, t) = \frac{\Phi_0}{(\pi\hat{t})^{1/2}} \frac{\zeta}{x^2} G(\zeta), \qquad \zeta = \frac{x^2}{\delta^2 + z^2/\hat{t}} \tag{9.28}$$

where G is Kummer's hypergeometric function, $G(\zeta) = M\left(1, \frac{1}{2}, -\zeta\right)$. Now expressions (9.26) and (9.28) seem to contradict (9.19), which predicts that the angular momentum decays as $\exp(-t/2\tau)$. However, (9.28) has an interesting property. For $t \gg \tau$, the global angular momentum, H_y, is

$$H_y = \frac{4\Phi_0\delta^2}{\pi^{1/2}} \int_0^\infty \left(1 + x^2\right)^{-1/2} \int_0^\infty \zeta^{-1/2} G(\zeta) d\zeta dx$$

This integrates to zero, since $\int_0^\infty \zeta^{-1/2} G(\zeta) d\zeta = 0$. It would appear, then, that the structure of the flow at large times is such that the angular momentum is zero. The reason for this can be seen from Figure 9.7, which shows the flow for $t \gg \tau$ (the structure of the flow at low N is also shown). Regions of reverse flow occur either side of the centre line of the vortex. This reverse flow has a magnitude which is just sufficient to cancel the angular momentum of the primary eddy.

We conclude, therefore, that the structure of the flow for large t is long and streaky, comprising vortex sheets of alternating sign. In short, the vorticity diffuses along the **B**-lines in accordance with (9.22) while simultaneously adopting a layered structure which has zero net angular momentum, thus satisfying (9.19).

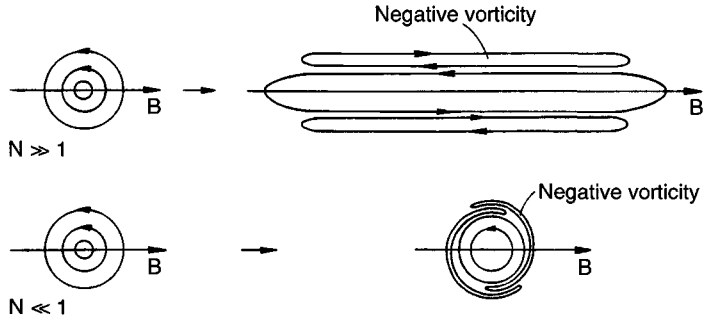

Figure 9.7 Magnetic damping of a transverse vortex at low and high N: a schematic view.

9.4.3 Damping of parallel vortices

We now consider a vortex whose axis is aligned with **B**. For simplicity, we restrict ourselves to axisymmetric vortices, described in terms of cylindrical polars (r, θ, z) with **B** parallel to z. We shall neglect viscosity and assume that initial conditions are such that the integral of the angular momentum converges at $t = 0$. Aspects of this problem have been touched upon in Chapter 5, Section 2.3

Suppose we have an isolated region of intense swirl, of characteristic radius δ, in an otherwise quiescent liquid. We may uniquely define the instantaneous state of the flow using just two scalar functions: Γ, the angular momentum, and Ψ, the Stokes streamfunction. These are defined through the expressions

$$\mathbf{u} = \mathbf{u}_\theta + \mathbf{u}_p = (\Gamma/r)\hat{\mathbf{e}}_\theta + \nabla \times [(\Psi/r)\hat{\mathbf{e}}_\theta] \tag{9.29}$$

$$\nabla_*^2 \Psi = \frac{\partial^2 \Psi}{\partial z^2} + r\frac{\partial}{\partial r}\left(\frac{1}{r}\frac{\partial \Psi}{\partial r}\right) = -r\omega_\theta \tag{9.30}$$

Note that the velocity has been divided into azimuthal and poloidal components. The Lorentz force, which is linear in **u**, may be similarly divided, giving

$$\mathbf{F}_p = -\frac{u_r}{\tau}\hat{\mathbf{e}}_r = \frac{1}{r\tau}\frac{\partial \Psi}{\partial z}\hat{\mathbf{e}}_r, \qquad F_\theta = -\frac{1}{\tau}\frac{J_r}{\sigma B} = \frac{1}{r\tau}\frac{\partial \phi}{\partial z} \tag{9.31, 9.32}$$

Here $\sigma B\phi$ is the Stokes streamfunction for $\mathbf{J}_p$ which, by virtue of Ohm's law, is related to Γ by

$$\nabla_*^2 \phi = -\partial \Gamma/\partial z \tag{9.33}$$

The governing equations for Γ and Ψ are the azimuthal components of the momentum and vorticity equations, respectively (Davidson, 1995):

$$\frac{D\Gamma}{Dt} = \frac{1}{\tau}\frac{\partial \phi}{\partial z} = -\frac{1}{\tau}\frac{\partial^2}{\partial z^2}\left[\nabla_*^{-2}\Gamma\right] \tag{9.34}$$

$$\frac{D}{Dt}\left(\frac{\omega_\theta}{r}\right) = \frac{1}{r^4}\frac{\partial \Gamma^2}{\partial z} - \frac{1}{r^2\tau}\frac{\partial^2}{\partial z^2}\left[\nabla_*^{-2}(r\omega_\theta)\right] \tag{9.35}$$

Note the appearance of the pseudo-diffusion terms. We might anticipate that angular momentum propagates along the magnetic field lines, and we shall see that this is substantially correct.

We shall now draw some general conclusions from (9.34) and (9.35). First, it is apparent from (9.34) that the global angular momentum is conserved:

$$I_\Gamma = \int \Gamma dV = \text{constant}. \tag{9.36}$$

This is a special case of (9.15a) and may be contrasted with the angular momentum of a transverse vortex. Second, for confined domains the kinetic energy of the flow has a lower bound. Specifically, the Schwarz inequality gives

$$E_\theta \geq I_\Gamma^2 \Big/ 2\int r^2 dV \tag{9.37}$$

where E_θ is the energy of the azimuthal component of motion. Third, as noted earlier, any initial condition (in a confined domain) must evolve to a steady state of the form $(0, u_\theta(r), 0)$. In fact, this is true for any value of N, and follows directly the energy equation (9.3). That is, we know that the flow eventually reaches a steady state with non-zero E_θ, at which time the Joule dissipation must vanish. Yet from (9.31) $\rightarrow$ (9.33) we know that $|\mathbf{J}|$, and hence the dissipation disappears only when u_r and $\partial\Gamma/\partial z$ are both zero. This is a special case of the three-dimensional result discussed in Section 4.1 of this chapter.

For infinite domains (9.37) does not apply. However, we can still use conservation of angular momentum to determine the manner in which the flow evolves. From (9.4a) we have

$$\frac{dE}{dt} \sim -\left(\frac{\delta}{l_z}\right)^2 \frac{E}{\tau} \tag{9.38}$$

Thus the total energy declines as

$$E \sim E_0 \exp\left[-\int_0^{\hat{t}} (\delta/l_z)^2 d\hat{t}\right] \tag{9.39}$$

If angular momentum is to be conserved, then there are only two ways in which this decrease in energy can be accommodated. Either l_z increases with time to reduce the dissipation, thus avoiding the exponential decline in energy, or else the angular momentum centrifuges itself radially outward, allowing the energy to decline despite the conservation of I_Γ. We shall see that axial spreading of angular momentum is typical of high-N flows, while the radial spreading of angular momentum is characteristic of low-N flows.

Let us now consider separately the limits of high and low N. When N is large, the azimuthal and poloidal motions are decoupled. Specifically, N is of the order of $l/u\tau$, so that when N is large the kinetic energy exchange between u_θ and $\boldsymbol{u}_p$ (via the centrifugal force) is negligible by comparison with the Joule dissipation. If the energy of the poloidal flow, E_p, is initially small (of the order of $N^{-1}E_\theta$), it remains small. The flow is then governed by the simple linear equation

$$\frac{\partial \Gamma}{\partial t} = -\frac{1}{\tau}\frac{\partial^2}{\partial z^2}\left[\nabla_*^{-2}\Gamma\right] \tag{9.40}$$

We expect, therefore, that any localised region of swirl will diffuse along the magnetic field lines at a rate determined by

$$l_z \sim \delta(t/\tau)^{1/2} \tag{9.41}$$

We may confirm this by taking the Fourier transform of (9.40). Suppose that the flow is unbounded and let U be the first-order Hankel-cosine transform of u_θ.

$$U(k_r, k_z) = 4\pi \int_0^\infty \int_0^\infty \Gamma(r, z) J_1(k_r r) \cos(k_z z) r dr dz \tag{9.42}$$

Then (9.40) shows that U decays as

$$U = U_0 e^{-(\cos^2\phi)\hat{t}}, \qquad \cos\phi = k_z/k \tag{9.43}$$

As before, $\hat{t}$ is the dimensionless time t/τ, U_0 represents the initial condition, and k is the magnitude of $\boldsymbol{k}$. We can now determine Γ by taking the inverse transform. For large times this is (Davidson, 1997)

$$\Gamma(\hat{t} \to \infty) = \frac{r\hat{t}^{-1/2}}{2\pi^2} \int_0^\infty \int_0^\infty [kU_0(k, k_z)] e^{-q^2} J_1(kr) \cos\left(kqz/\hat{t}^{1/2}\right) k dk dq \tag{9.44}$$

This confirms that, for large values of t, the distribution of angular momentum is of the form

$$\Gamma(\mathbf{x}, t) = (t/\tau)^{-1/2} F\big(r, z/(t/\tau)^{1/2}\big) \tag{9.45}$$

Note the similarity between (9.45) and the evolution of ψ for two-dimensional transverse vortices. As expected, the angular momentum propagates along the z-axis at a rate governed by (9.41), but decays according to $u_\theta \sim (t/\tau)^{-1/2}$. The energy of the vortex therefore declines at a rate

$$E \sim (t/\tau)^{-1/2} \tag{9.46}$$

which is exactly the same as for a transverse vortex.

By way of an example, suppose that, at $t = 0$, we have a spherical blob of swirling fluid, so that our initial condition is

$$\Gamma_0(r, z) = \Omega r^2 \exp\big[-\big(r^2 + z^2\big)/\delta^2\big]$$

Then it is readily confirmed that (9.44) gives

$$u_\theta\big(\hat{t} \to \infty\big) = \Omega\delta\hat{t}^{-1/2}\frac{3}{4}\pi^{1/2}\left(\frac{\delta}{r}\right)^4 \zeta^{5/2} H(\zeta), \qquad \zeta = \frac{r^2}{\delta^2 + z^2/\hat{t}} \tag{9.47}$$

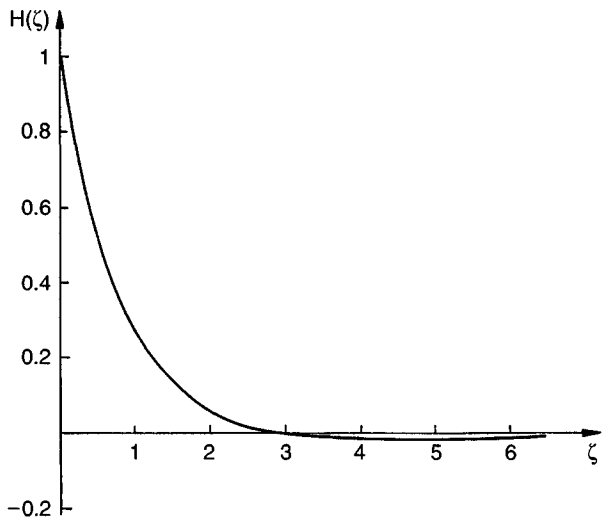

Figure 9.8 Magnetic damping of a parallel vortex at high N. $H(\zeta)$ is the distribution of swirl with radius at large t. Note the reverse rotation at large radii.

Here $H(\zeta)$ is the hypergeometric function $H(\zeta) = M(\frac{5}{2}, 2, -\zeta)$. The shape of $H(\zeta)$ is shown in Figure 9.8. Curiously, at large ζ, the function H becomes negative ($H \sim -\zeta^{-5/2}/2\pi^{1/2}$), so that the primary vortex is surrounded by a region of counter-rotating fluid. This may be attributed to the way in which the induced currents recirculate back through quiescent regions outside the initial vortex (see later). We conclude, therefore, that the asymptotic structure of a vortex aligned with **B** is as shown schematically in Figure 9.9. It is cigar-like in shape, and quite different in structure to the transverse vortex shown in Figure 9.7. Curiously, though, despite the fact that the two classes of vortices adopt very different structures, their energies both decay as $(t/\tau)^{-1/2}$

The mechanism for the propagation of angular momentum is shown in Figure 9.10. The term $\mathbf{u}_\theta \times \mathbf{B}$ tends to drive a radial current, J_r. Near the centre of the vortex, where the axial gradient in Γ is small, this is counter-balanced by an electrostatic potential, Φ, and so almost no current flows. However, near the top and bottom of the vortex, the current can return through regions of small or zero swirl. The resulting inward flow of current above and below the vortex gives rise to a positive azimuthal torque which, in turn, creates positive angular momentum in previously stagnant regions. Notice also that regions of reverse flow form in an annular zone surrounding the initial vortex where F_θ is negative.

We now turn our attention to the case where N is low. Since the Joule dissipation is negligible on time scales of the order of l/u, the flow evolves

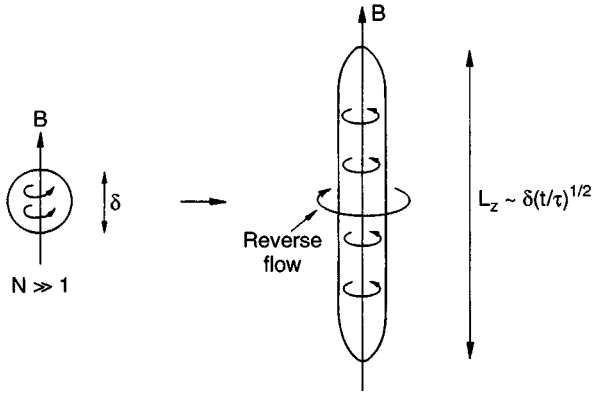

Figure 9.9 Magnetic damping of a parallel vortex at high N. The figure shows schematically the structure of the flow at large t.

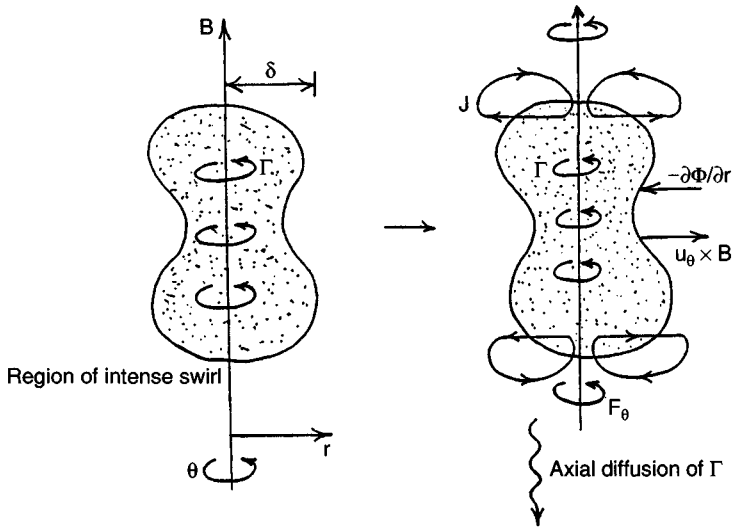

Figure 9.10 Magnetic damping of a region of intense swirl: (a) the initial swirl distribution; (b) the axial diffusion of angular momentum.

in accordance with the undamped Euler equations. Our initial blob of swirling fluid, which is centrifugally unstable, will centrifuge itself radially outward. This occurs through the angular momentum organizing itself into one or more ring-shaped vortices. These propagate radially outward with the characteristic mushroom-like structure of a thermal plume. This is shown schematically in Figure 9.11.

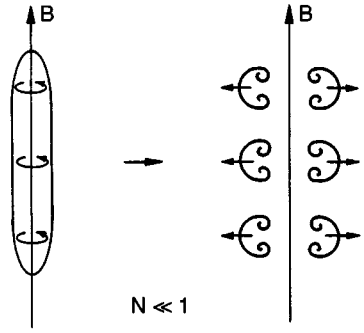

Figure 9.11 Magnetic damping of a parallel vortex at low N. The vortex will disintegrate through hoops of swirling fluid centrifuging themselves radially outward.

9.4.4 Implications for low-R_m turbulence

Consider a homogeneous, low-R_m turbulent flow which is freely evolving in a uniform magnetic field. Suppose that the interaction parameter, $N = \sigma B_0^2 l/\rho u$, is large when based on the integral scale of the turbulence. Then inertia may be neglected as far as the large (energy containing) eddies are concerned and, since **J** is linear in **u**, these eddies are governed by the (linear) equation of motion,

$$\rho \frac{\partial \mathbf{u}}{\partial t} = -\nabla(P) + \mathbf{J} \times \mathbf{B}_0$$

In view of the linearity of this equation, we might regard the turbulence as an ensemble of independent eddies, some of which are initially aligned with the field $\mathbf{B}_0$ and some of which are non-aligned. These eddies will evolve in a manner not unlike those described in the previous sections. Vortices whose rotation axis is aligned with the magnetic field will develop into long, columnar structures. Those which are perpendicular to $\mathbf{B}_0$ will develop into sheet-like structures consisting of thin, interwoven layers of oppositely signed vorticity, the dominant velocity being $\mathbf{u}_{//}$. Both types of vortices will lose their kinetic energy at a rate $E \sim (t/\tau)^{-1/2}$. Thus we might expect two generic types of structures to emerge: columns and sheets (Figure 9.12). Moreover, since $\mathbf{u}_\perp$ is prefer-

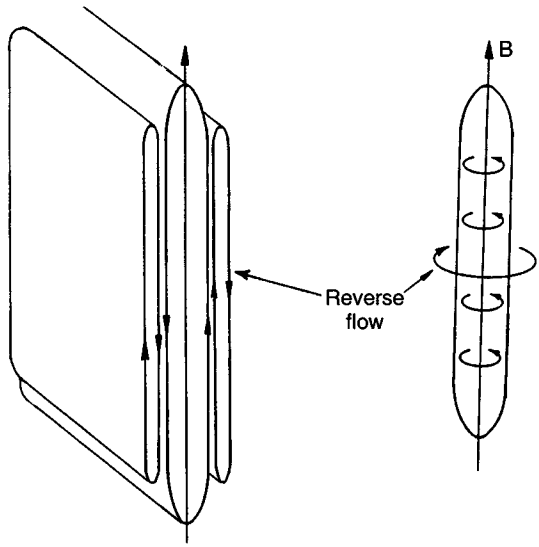

Figure 9.12 Typical flow structure in high-N turbulence.

entially destroyed in the sheets, we might expect $\mathbf{u}_{//}^2/\mathbf{u}_{\perp}^2$ to increase as the flow evolves from some initial isotropic state. In fact, this is precisely what is observed in numerical simulations. The ratio $\mathbf{u}_{//}^2/\mathbf{u}_{\perp}^2$ tends to a value of 2 at large times (as predicted by Moffatt, 1967), as long as N remains large.

9.5 Damping of Natural Convection

We have already discussed the damping of natural convection in the context of Rayleigh–Benard convection. Here we shall consider a different configuration, which is particularly important in the casting of aluminium. We shall examine natural convection in an axisymmetric pool, driven by a difference in temperature between the surface and the sides of the pool. We consider first convection in the absence of a magnetic field, and then examine the influence of an imposed field.

9.5.1 Natural convection in an aluminium ingot

Consider a cavity which is filled with liquid metal and has maximum radius R. Suppose that the walls of the cavity are maintained at a reference temperature, T_M, while the upper surface of the metal is maintained at the higher temperature of $T_M + \Delta T$. Then natural convection will ensure that the liquid metal flows as shown in Figure 9.13, falling at the walls and rising up through the core. The problem just specified is a zero-order model of the casting of aluminium. Figure 9.14 is a simple representation of an aluminium caster. In essence, a solid ingot is slowly withdrawn from a liquid metal pool, the pool being continuously replenished from above. It is well known that buoyancy-driven flow arises during this process, and that this flow has a substantial influence on the metallurgical structure of the solid, affecting both the grain size and the macro-segregation within the ingot. There is considerable motivation then to understand how the magnitude and distribution of the flow field varies with, say, the pool size or superheat ΔT.

The Reynolds number for the flow is assumed to be large, and the flow is taken to be laminar (although in practice it is likely to be turbulent). The Prandtl number is, of course, much less than one. We shall invoke the Boussinesq approximation, in which the velocity field remains solenoidal. The equation of motion for the liquid metal is then

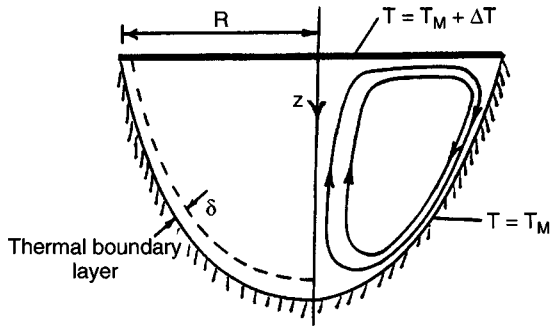

Figure 9.13 Thermally driven flow in a cavity. The upper surface is maintained at temperature $T_M + \Delta T$ and the walls at the lower temperature of T_M. Cold fluid falls near the walls.

$$\frac{D\mathbf{u}}{Dt} = -\nabla\left(\frac{P}{\rho}\right) - g\beta(T - T_M)\,\hat{\mathbf{k}} + \nu\nabla^2\mathbf{u} \tag{9.48}$$

and the corresponding transport equations for vorticity and heat are, in cylindrical polar coordinates,

$$\frac{D}{Dt}\left(\frac{\omega_\theta}{r}\right) = g\beta\frac{1}{r}\frac{\partial T}{\partial r} + \nu\left\{\nabla^2\left(\frac{\omega_\theta}{r}\right) + \frac{2}{r}\frac{\partial}{\partial r}\left(\frac{\omega_\theta}{r}\right)\right\} \tag{9.49}$$

$$\frac{DT}{Dt} = \alpha\nabla^2 T \tag{9.50}$$

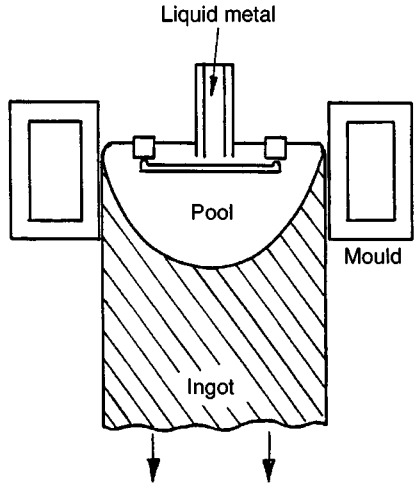

Figure 9.14 Casting of aluminium.

Here α is the thermal diffusivity, β the expansion coefficient and ν the kinematic viscosity.

We shall denote the thickness of the thermal boundary layer on the cavity wall by δ, and use subscripts c and b to indicate parameters inside and outside the thermal boundary layer, respectively. Thus, for example, the temperature field in the core is T_c, while the velocity field in the thermal boundary layer is $\mathbf{u}_b$. We now show that the core of the melt is thermally stratified: that is

$$T_c \approx T_c(z) \tag{9.51}$$

To this end it is useful to integrate (9.48) around any closed streamline to give

$$g\beta \oint (T - T_M)dz = \nu \oint \nabla^2 \mathbf{u} \cdot d\mathbf{l} \tag{9.52}$$

This states that the energy gained by a fluid particle, by virtue of the buoyancy force, must be diffused or dissipated out of the particle by shear. However, in view of the smallness of ν, the second integral would appear to be vanishingly small. Nevertheless, there are three ways in which we could guarantee that all streamlines satisfy (9.52). These are:

(a) $\mathbf{u}$ scales as l/ν;
(b) *all* streamlines pass through a singular region, where the velocity gradients scale as $\nu^{1/2}$;
(c) the core is thermally stratified, in accordance with (9.51).

We may eliminate the first of these possibilities, as it implies very large velocities. We are left, therefore, with options (b) and (c). There are two possible singular regions which are candidates for option (b). One is the viscous boundary layer on the cavity wall, and the other is the region at the bottom of the cavity where the wall jets collide. However, to pass through the dissipative region at the base of the cavity, a streamline must first have entered the wall jet. Consequently, option (b) is equivalent to saying that all streamlines must pass through the thermal boundary layer.

In fact, we may show that *both* (b) and (c) hold true. That is, the core is thermally stratified, and all the streamlines pass through the thermal boundary layer. The argument proceeds by showing that if either one of (b) or (c) holds, then the other must follow. The argument is as follows. Suppose (c) holds true, but (b) does not. Then (9.50) applied to the core requires that

$$u_{zc}T_c'(z) = \alpha T_c''(z) \tag{9.53}$$

This implies that u_{zc} is a function of z only, and hence from continuity, u_{rc} is a linear function of r. This, in turn, implies that all streamlines will pass out of the core and into the boundary layer. Consequently, (b) must hold true after all.

We may also show that the converse is true by using scaling arguments. For convenience, we shall take the datum for temperature to be T_M. Also, let L_T be the axial length-scale in the core. Then (9.48) applied in the boundary layer requires that

$$\frac{u_{zb}^2}{L_T} \sim g\beta T_c$$

In addition, if all the streamlines pass through the thermal boundary layer, continuity requires that

$$u_{zc} \sim \frac{u_{zb}\delta}{R}$$

These estimates show that, in the core,

$$\mathbf{u} \cdot \nabla(\omega_\theta) \sim g\beta \frac{T_c\delta^2}{(RL_T^2)}$$

from which we deduce

$$\frac{\partial T_c}{\partial r} \sim \frac{T_c}{R}\left(\frac{\delta}{L_T}\right)^2$$

Consequently, provided $L_T \gg \delta$ (and we shall see that this is indeed the case), the core is thermally stratified according to

$$T_c = T_c(z)\left\{1 + 0\left(\frac{\delta}{L_T}\right)^2\right\}$$

Thus it appears that the flow satisfies both conditions (b) and (c) (Davidson & Flood, 1994)

We might speculate, then, that the flow field is as shown in Figure 9.15. There is a relatively quiescent, stratified core, bounded by thermal wall jets, within which the temperature adjusts from the core distribution to the wall temperature. The rôle of the wall jets is to carry hot fluid away from the top surface and allow it to cool on the colder, curved boundary. If we now allow for a small inflow, u_0, at the top surface, then some additional (open) streamlines will start at the surface and leave through the cavity wall. Since these additional lines cannot cross the recirculating

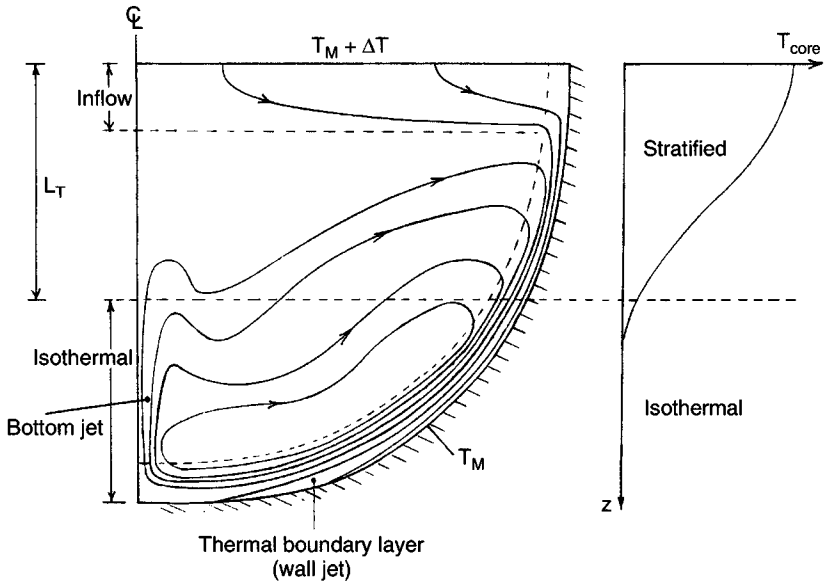

Figure 9.15 General structure of the flow field.

streamlines, they must be diverted into the wall jet and pass down behind the closed streamlines. Eventually, they will leave the flow field in (predominantly) the lower half of the cavity. We shall show later that the axial length-scale for the decay of core temperature, L_T, typically has a value of $\sim R/6$. (This follows from general scaling arguments.) Consequently, the stratified region occupies only the upper part of the pool. Below this, we have an isothermal melt, with $T = T_M$.

Let us now determine the scaling laws for L_T, u_c, u_b and δ. We have four equations to be satisfied. First (9.48) and (9.50) demand that, in the boundary layer,

$$u_b^2/L_T \sim g\beta\Delta T, \qquad u_b/L_T \sim \alpha/\delta^2 \qquad (9.54, 9.55)$$

Next, (9.53) and continuity yield

$$u_c \sim \alpha/L_T, \qquad u_c R \sim u_b \delta \qquad (9.56, 9.57)$$

If we introduce the dimensionless parameter

$$Gr = \frac{g\beta R^3 \Delta T}{\alpha^2}$$

then (9.54) to (9.57) give us the required scaling laws:

$$L_T \sim (Gr)^{-1/7} R, \qquad \frac{\delta}{R} \sim (Gr)^{-2/7} \tag{9.58, 9.59}$$

$$u_b \sim \frac{\alpha}{R}(Gr)^{3/7}, \qquad u_c \sim \frac{\alpha}{R}(Gr)^{1/7} \tag{9.60, 9.61}$$

In casting, typical parameter values are $Gr = 10^6$, $\alpha = 4 \times 10^{-5}\,\mathrm{m}^2/\mathrm{s}$ and $R = 0.3\,\mathrm{m}$, from which $L_T \sim 0.14R$, $\delta \sim 0.02R$, $u_c \sim 1\,\mathrm{mm/s}$ and $u_b \sim 50\,\mathrm{mm/s}$. The inlet velocity is typically of the order of $u_0 = 1\,\mathrm{mm/s}$, which is similar to u_c but much less than u_b. These scaling laws have been tested against experimental data and numerical simulations and found to be reasonably accurate. A typical numerical simulation, taken from Davidson & Flood (1994), is shown in Figure 9.16.

It is widely believed that this natural convection pattern is detrimental to the ingot structure, causing inhomogeneities in chemical composition. The argument is that small (snow-flake-like) crystals, which nucleate near the boundaries, become caught up in the wall jets and are swept down to the base of the pool. For thermodynamic reasons, the crystals which form near the top of the pool tend to be depleted in the alloying elements, and it is these crystals which get caught up in wall jets and end up at the centre of the ingot. Two radically different solutions to this problem have been proposed. One is magnetic stirring, which was discussed in the previous chapter, and the other is magnetic damping.

9.5.2 Magnetic damping in an aluminium ingot

It is evident that the driving force for natural convection is concentrated near the top of the pool and within the thermal boundary layer. Since the sides of the pool are approximately vertical at this point, it seems natural to use a (predominantly) horizontal magnetic field to suppress the motion. The required magnitude of the imposed field may be determined as follows. If the Lorentz force is to reduce the velocity significantly it must be as large as the buoyancy force, and so

$$u/\tau \sim g\beta\Delta T, \qquad \tau^{-1} = \sigma B^2/\rho$$

This implies that u_b is of the order of $u_b \sim (g\beta\Delta T)\tau$. If the damping is to be effective then u_b should be less than the estimate (9.60), and so we find that the minimum acceptable value of $|\mathbf{B}|$ is given by

$$\sigma B_{\min}^2 R^2/\rho\alpha \sim (Gr)^{4/7} \tag{9.62}$$

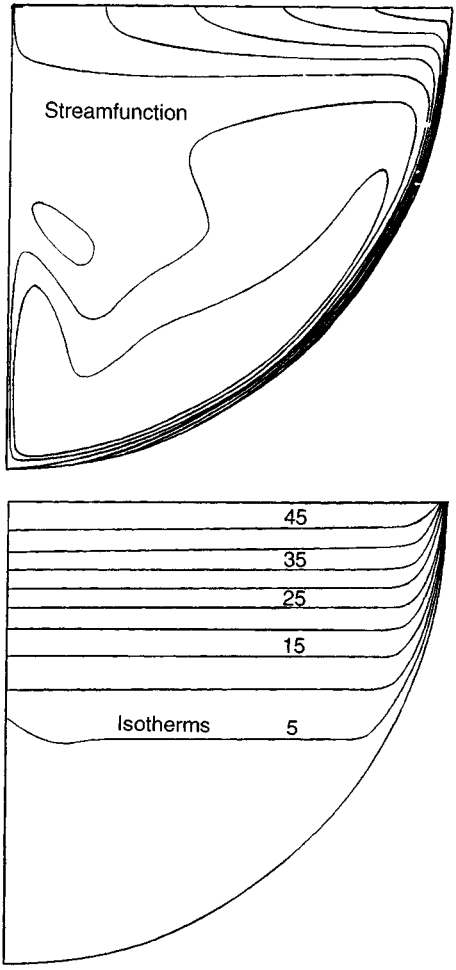

Figure 9.16 Computed isotherms and streamfunction for $\Delta T = 50°C$.

Examples

9.1 Consider the one-dimensional jet shown in Figure 9.3. Suppose that the jet is driven by buoyancy and that $N \gg 1$, $\alpha \to 0$. Show that, at large times,

$$u \sim g\beta\tau\Delta T(t/\tau)^{1/2} F\left(\frac{z}{(t/\tau)^{1/2}}, x\right)$$

where ΔT is a measure of the temperature difference driving the flow.

9.2 Consider the axisymmetric vortex discussed in Section 9.4.3. Show that the energies of the azimuthal and poloidal motions are governed by

$$\frac{dE_\theta}{dt} = -\int \frac{u_\theta^2}{r} u_r dV - \frac{1}{\tau}\int (\nabla\phi)^2 \frac{dV}{r^2}$$

$$\frac{dE_p}{dt} = +\int \frac{u_\theta^2}{r} u_r dV - \frac{1}{\tau}\int u_r^2 dV$$

Now show that these are compatible with the overall energy balance 9.4(a). When N is small, estimate the time taken for the structures shown in Figure 9.11 to emerge.